

Mutual annihilation of counter-rotating spiral waves induced by electric fields

Ying-Qi Liu(刘瑛琦), Yi-Peng Hu(胡义鹏), Qian-Ming Ding(丁钱铭), Ying Xie(谢盈), and Ya Jia(贾亚)
Citation: Chin. Phys. B, 2025, 34 (**12**): 120505. DOI: 10.1088/1674-1056/ae0561
http://cpb.iphy.ac.cn; http://iopscience.iop.org/cpb

What follows is a list of articles you may be interested in

Dynamical behaviors of a multifunctional neural circuit

Xiao-Hong Gao(高晓红), Kai-Long Zhu(朱凯龙), and Fei-Fei Yang(杨飞飞)
Chin. Phys. B, 2025, 34 (**9**): 090503. DOI: 10.1088/1674-1056/ae001b

Current bifurcation, reversals and multiple mobility transitions of dipole in alternating electric fields

Wei Du(杜威), Kao Jia(贾考), Zhi-Long Shi(施志龙), and Lin-Ru Nie(聂林如)
Chin. Phys. B, 2023, 32 (**2**): 020505. DOI: 10.1088/1674-1056/ac7dbe

Applying a global pulse disturbance to eliminate spiral waves in models of cardiac muscle

Jian Gao(高见), Changgui Gu(顾长贵), and Huijie Yang(杨会杰)
Chin. Phys. B, 2021, 30 (**7**): 070501. DOI: 10.1088/1674-1056/abf553

Effects of abnormal excitation on the dynamics of spiral waves

Min-Yi Deng(邓敏艺), Xue-Liang Zhang(张学良), Jing-Yu Dai(戴静娱)
Chin. Phys. B, 2016, 25 (**1**): 010504. DOI: 10.1088/1674-1056/25/1/010504

The effect of cellular aging on the dynamics of spiral waves

Deng Min-Yi (邓敏艺), Chen Xi-Qiong (陈茜琼), Tang Guo-Ning (唐国宁)
Chin. Phys. B, 2014, 23 (**12**): 120503. DOI: 10.1088/1674-1056/23/12/120503

SPECIAL TOPIC — Biophysical circuits: Modeling & applications in neuroscience

Mutual annihilation of counter-rotating spiral waves induced by electric fields

Ying-Qi Liu(刘瑛琦), Yi-Peng Hu(胡义鹏), Qian-Ming Ding(丁钱铭), Ying Xie(谢盈), and Ya Jia(贾亚)[†]

Department of Physics, Central China Normal University, Wuhan 430079, *China*

(Received 5 July 2025; revised manuscript received 10 September 2025; accepted manuscript online 10 September 2025)

Spiral waves, as a typical self-organized structure with chiral characteristics, are widely found in excitable media such as cardiac tissues, chemical reactions, and neural networks. Based on the FitzHugh–Nagumo model, we investigated the mechanisms underlying the effects of direct current electric fields (DCEF), alternating current electric fields (ACEF), and polarized electric fields (PEF) on the interaction and annihilation processes of counter-rotating spiral waves. We found that in a direct current electric field, the drift direction of the spiral wave is determined jointly by its chirality and the electric field direction, which allows selective attraction or repulsion. In an alternating current electric field, the annihilation behavior of spiral waves can be influenced by the phase and intensity of the electric field, where a specific range of parameters induces resonance drift and eventual annihilation. On the other hand, the polarized electric field exhibits a more complex modulation capability on spiral waves: the trajectory and annihilation efficiency of spiral waves can be regulated by both the intensity and phase of the polarized electric field. These results reveal the potential feasibility of regulating multichiral spiral waves through multiple electric fields, providing theoretical insight for the control of spiral waves in relevant systems.

Keywords: spiral waves, electric fields, chirality

PACS: 05.65.+b, 47.54.−r

DOI: 10.1088/1674-1056/ae0561 **CSTR:** 32038.14.CPB.ae0561

1. Introduction

Excitable media are a widely occurring class of nonequilibrium systems in nature that play an important role in a variety of fields, including chemistry, physics, and biology. Among them, spiral waves[1,2] are a typical spatiotemporal self-organized structure widely found in systems such as cardiac tissue,[3,4] CO-catalyzed oxidation reactions on platinum surfaces,[5] and the Belousov–Zhabotinsky (BZ) reaction.[6,7] Spiral waves modulate the mode of excitation propagation in space, and their dynamical characteristics largely determine the evolution of excitable media. In the heart, for example, stationary rotating spiral waves can produce monomorphic tachycardia,[8] whereas their rupture may lead to ventricular fibrillation,[9] one of the main sources of sudden death. When spiral waves drift through the heart, they may also induce a more complex arrhythmia called polymorphic ventricular tachycardia.[10] Meanwhile, the dynamics of various types of networks have received considerable attention.[11,12] The dynamical behaviors of spiral waves have been widely studied based on the kinetic properties of individual neurons[13–15] and in diverse networks composed of multiple neuron models[16,17] to investigate the effects of factors such as electromagnetic action on spiral waves.[18] In recent years, the important role of adaptive synaptic currents in regulating spiral wave behavior has also attracted extensive attention.[19] In addition, noise likewise affects the network,[20,21] which in turn alters the dynamical behavior of spiral waves.[22–24]

Spiral wave drift is an important kinetic behavior, and by driving the wave to move, it is possible to modulate the location of spiral waves or even eliminate them. In cardiac tissue, light can induce alterations in wave dynamics, leading to drift of spiral waves,[25–27] reverse chirality,[28] and triggering of electrical turbulence.[29,30] However, optogenetic signals act only on the surface of the heart, whereas the ventricular wall is thicker, and the actual thickness of cardiac tissue leads to the attenuation of blue light during irradiation, thus limiting the deep effect of photocontrol techniques. In addition, spiral wave drift can occur in magnetically sensitive media under magnetic flux[31] or temperature gradient terms.[32] A spiral wave has been demonstrated to drift along both the parallel and perpendicular directions of an applied direct current electric field,[33,34] with the direction of drift determined by the wave's chiral characteristics. Spiral waves may drift in the opposite direction in weakly excitable media, but they tend to follow the electric field in highly excitable media.[35] Furthermore, in the BZ reaction, the spiral wave undergoes directional drift when an alternating current electric field with a frequency twice that of the spiral is applied.[36] The polarized electric field with chirality was theoretically postulated[37] based on the rotational symmetry of the spiral wave around its center,

[†]Corresponding author. E-mail: jiay@ccnu.edu.cn

© 2025 Chinese Physical Society and IOP Publishing Ltd. All rights, including for text and data mining, AI training, and similar technologies, are reserved.

and the resonant drift behavior under the polarized electric field was examined. When the frequency of the polarized electric field is double that of the spiral wave, directional drift of the spiral has been observed.[38] By adding a gradient term to the spatial operator, numerical simulations can replicate similar results. Prior research has thoroughly examined the drift behavior of spiral waves in direct current and alternating current electric fields,[39] as well as their drift characteristics in circularly polarized electric fields.[37] Moreover, experimental results confirm that the dynamics of spiral waves are altered under the action of a polarized electric field.[40–46]

Spiral waves are a typical self-organized structure with a well-defined chiral character, where the direction of rotation (clockwise or counterclockwise) corresponds to a specific topological charge (-1 or $+1$).[47] Chirality is an asymmetric property that is prevalent in several scientific fields, including particle physics and biological systems.[43] Several methods exist to realize the selection of spiral wave chirality. For example, circularly polarized electric fields can break chiral symmetry by selecting spiral waves with a specific chirality[48] and verify it experimentally.[43] In cardiac media, the chirality of a spiral wave can be determined by the relative position between the obstacle and the pacing point.[42] The reaction-diffusion system has mirror symmetry, and counterclockwise and clockwise spiral waves are physically identical. However, when external perturbations such as electric fields or geometric asymmetries are incorporated into the system, this mirror symmetry may be broken, providing new approaches for spiral wave manipulation.

Although the above studies have made considerable progress in understanding the response mechanisms of spiral waves, most current work focuses on the response properties of a single chiral spiral wave under an electric field. Exploration of the interactions and annihilation processes between coexisting clockwise and counterclockwise chiral spirals remains relatively limited. When two counter-rotating spiral waves are close to each other, they can either attract and annihilate or repel, depending on their separation distance, initial phases, and rotational chirality.[49–51] In real systems, multiple spiral waves of opposite chirality often coexist, and their interactions are crucial for the evolution of the overall system. In particular, inducing two counter-rotating spiral waves to undergo mutual annihilation under an electric field is an important issue that has yet to be deeply explored.

In this paper, based on the FitzHugh–Nagumo (FHN) model, we investigate the modulation mechanisms of different types of electric fields (direct current electric fields (DCEF), alternating current electric fields (ACEF), and polarized electric fields (PEF)) on the mutual annihilation behavior of two counter-rotating spiral waves. Section 2 describes the adopted network model, the form of the electric field, and the statistical methods used. Section 3 analyzes the effects of three types of electric fields on the dynamics of spiral waves in turn: Subsection 3.1 focuses on the role of direct current electric fields; Subsection 3.2 explores alternating current electric fields; and Subsection 3.3 investigates the modulation capabilities of polarized electric fields. Finally, Section 4 summarizes the paper.

2. Models and methods

2.1. FitzHugh–Nagumo model

To describe the drift behavior of spiral waves in the presence of an electric field $\boldsymbol{E}$, we use a two-variable reaction-diffusion model. It is a classical approach for describing pattern formation in reaction-diffusion systems and is particularly suitable for studying the dynamics of spiral waves.

In this paper, the FitzHugh–Nagumo (FHN) model is chosen as the dynamical framework for the reaction-diffusion system. The basic equations of the model can be expressed as

$$\begin{cases} \dfrac{\partial u}{\partial t} = \dfrac{u - u^3/3 - v}{\varepsilon} + D\left(\dfrac{\partial^2 u}{\partial x^2} + \dfrac{\partial^2 u}{\partial y^2}\right), \\ \dfrac{\partial v}{\partial t} = \varepsilon\,(u + \beta - \gamma v), \end{cases} \tag{1}$$

where u and v are fast and slow variables, respectively. The diffusion term $D\left(\frac{\partial^2 u}{\partial x^2} + \frac{\partial^2 u}{\partial y^2}\right)$ describes the coupling between a node and its neighboring nodes, and D is the diffusion constant. The parameter values used in this paper are $D = 1$, $\varepsilon = 0.22$, $\beta = 0.58$, $\gamma = 0.8$.

To study the dynamic behavior of spiral waves under an electric field, numerical methods are employed to discretize and solve the model. A uniform two-dimensional spatial region with a grid size of 300×300, a time step of $\Delta t = 0.01$, and a spatial step of $\Delta x = \Delta y = 0.3$ is used. The boundary conditions are no-flux, meaning the normal gradients of u and v at the boundaries are zero. When spiral waves approach the boundary, they do not pass through or disappear but drift along it. In this study, spiral waves generally annihilate in the intermediate region, so boundary effects on their dynamics are minimal.

Without an applied electric field, spiral waves spontaneously rotate around a fixed center. In this paper, the left spiral wave center is set at (130, 152) and the right spiral wave center at (170, 152), with a polar coordinate system established using the horizontal direction as the reference axis. The initial positions of the spiral tips are connected to their respective centers, and their polar angles relative to the reference point are calculated: $\theta_i = \tan^{-1}(\mathrm{d}y/\mathrm{d}x)$, providing the initial phase angles of the left and right spiral tips. By recording tip positions over time, different combinations of initial phases under zero electric field can be obtained, forming a basis for analyzing their subsequent evolution.

In this study, spiral waves of opposite chirality are considered as the subjects of study. Initially, the left spiral wave rotates counterclockwise and the right spiral wave rotates clockwise. Their dynamic behavior under various electric field conditions, including tip trajectories, the annihilation process, and the system's overall dynamics, is analyzed via numerical simulations.

2.2. Electric fields

Previous studies on the effects of electric fields on spiral wave dynamics typically assume that the field is spatially uniform. Given the opposite chirality of spiral waves, it is meaningful to study their annihilation behavior under left-right symmetric electric fields. Based on the classical bivariate reaction-diffusion model, an electric-field coupling term $M\boldsymbol{E}\cdot\nabla u$ is incorporated into the original equations to describe the effects of different types of electric fields (DCEF, ACEF, and PEF) on spiral wave behavior

$$\begin{cases} \dfrac{\partial u}{\partial t} = \dfrac{u-u^3/3-v}{\varepsilon} + D\left(\dfrac{\partial^2 u}{\partial x^2}+\dfrac{\partial^2 u}{\partial y^2}\right) \\ \qquad\quad + ME_x\dfrac{\partial u}{\partial x} + ME_y\dfrac{\partial u}{\partial y}, \\ \dfrac{\partial v}{\partial t} = \varepsilon\left(u+\beta-\gamma v\right), \end{cases} \tag{2}$$

where $\boldsymbol{E}=(E_x,E_y)$ is the electric field and M is the ion mobility, set as $M=1$.

The electric field $\boldsymbol{E}=(E_x,E_y)$ is expressed as follows:

$$E_x=0,\ E_y=-E_0, \tag{3a}$$

$$E_x=0,\ E_y=E_0\cos(\omega t+\phi_0), \tag{3b}$$

$$\begin{cases} E_{x\mathrm{L}}=E_0\cos(\omega t+\phi),\ E_{x\mathrm{R}}=-E_0\cos(\omega t+\phi), \\ E_y=0, \end{cases} \tag{3c}$$

$$\begin{cases} E_{x\mathrm{L}}=E_0\cos(\omega t+\phi_1),\ E_{x\mathrm{R}}=-E_0\cos(\omega t+\phi_1), \\ E_y=E_0\cos(\omega t+\phi_2). \end{cases} \tag{3d}$$

Here, Eq. (3a) represents direct current electric fields, Eq. (3b) represents longitudinal alternating current electric fields, Eq. (3c) represents transverse alternating current electric fields, and Eq. (3d) represents polarized electric fields. E_0 is the electric field intensity, ω is the angular frequency, ϕ_0 is the initial phase of the longitudinal alternating current field, ϕ is the initial phase of the transverse alternating current field, and (ϕ_1,ϕ_2) is the initial phase combination of the polarized electric field.

2.3. Utilized statistical measures

We incorporate the following three statistics. The ordinal covariate A describes the difference between the maximum and minimum values of the membrane potential u in the system over the time scale T, characterizing the overall dynamical activity of the system, defined as

$$A=\frac{\sum_{i,j}^{N}\left(\langle u_{i,j,\max}\rangle_T-\langle u_{i,j,\min}\rangle_T\right)}{N}, \tag{4}$$

where N is the number of nodes (in this study, $N=90000$) and $\langle\,\rangle_T$ denotes the time average over the simulation. $A>0$ indicates the presence of spiral waves, whereas $A=0$ corresponds to their annihilation.

The synchronization error E measures the synchronization between different spatial points in the system, defined as

$$E=\left\langle\frac{1}{N(N-1)}\left[\sum_{i,j,i',j'}\left(u_{i,j}-u_{i',j'}\right)^2\right]^{\frac{1}{2}}\right\rangle_T. \tag{5}$$

A larger value of E indicates the presence of spiral waves, whereas $E=0$ implies their annihilation, meaning all nodes in the system are no longer excited.

The average membrane potential u_{mean} represents the overall state of the network and is defined as

$$u_{\mathrm{mean}}=\frac{1}{N}\sum_{i,j}^{N}\langle u_{i,j}\rangle_T. \tag{6}$$

2.4. Phase singularity identification method

The tip of a spiral wave is called a phase singularity (PS). By analyzing the two variables in numerical simulations, phase singularities can be calculated. Various membrane-potential-based methods have been proposed for PS identification, including the topological charge density method, the Jacobian determinant method, and the average flow velocity determinant-trace method.[52–54] In this paper, the topological charge density method is employed.

The trajectory of a spiral tip is usually computed using the two-variable phase method, with a fixed reference point in the system (e.g., $(u^*=0,v^*=0)$), and represented as

$$u_{x,y}(t)=u^*,\quad v_{x,y}(t)=v^*. \tag{7}$$

The solution of Eq. (7) can be expressed as $(x_{\mathrm{ps}}(t),y_{\mathrm{ps}}(t))$, where $x_{\mathrm{ps}}(t)$ and $y_{\mathrm{ps}}(t)$ denote the coordinates of the spiral tip. The phase variable $\varphi_{x,y}(t)$ at each point in the spiral wave is calculated as

$$\varphi_{x,y}(t)=\arctan 2\left[v-v^*,\ u-u^*\right]. \tag{8}$$

The topological properties of spiral tips are described by the topological charge n_{t}. Defining a closed curve C surrounding the spiral tip, the topological charge is given by[55]

$$n_{\mathrm{t}}=\frac{1}{2\pi}\oint_C\nabla\varphi\cdot\mathrm{d}\boldsymbol{l}. \tag{9}$$

A point is identified as a phase singularity when the phase variation around it is $\pm2\pi$, i.e., $n_{\mathrm{t}}=\pm1$. This arises because the medium wraps around the spiral tip throughout each stage of the activation-recovery cycle, whereas the phase at the tip itself is indeterminate.

According to Stokes' theorem, the above expression can be written in surface integral form

$$n_{\mathrm{t}} = \frac{1}{2\pi}\iint_S (\nabla\times\nabla\varphi)\cdot\boldsymbol{z}\,\mathrm{d}\sigma, \tag{10}$$

where S is the surface enclosed by C and $\mathrm{d}\sigma$ is the area element. The topological charge density is then expressed as

$$\rho_{x,y} = \frac{1}{2\pi}(\nabla\times\nabla\varphi)\cdot\boldsymbol{z}. \tag{11}$$

The spiral tip position $(x_{\mathrm{ps}}, y_{\mathrm{ps}})$ can be obtained using the Dirac delta function

$$\rho_{x,y} = n_{\mathrm{t}}\,\delta(x-x_{\mathrm{ps}})\,\delta(y-y_{\mathrm{ps}}). \tag{12}$$

In numerical calculations, for grid points (i,j),

$$\rho_{i,j}h^2 = \frac{1}{2\pi}\left[(\nabla\times\nabla\varphi)\cdot\boldsymbol{z}\right]_{i,j}h^2. \tag{13}$$

Using finite difference approximations, the phase gradient difference takes the form

$$\rho_{i+1/2,j+1/2}\,h^2 = \frac{1}{2\pi}\left(\frac{\dfrac{\varphi_{i+1,j+1}-\varphi_{i+1,j}}{h} - \dfrac{\varphi_{i,j+1}-\varphi_{i,j}}{h}}{h} - \frac{\dfrac{\varphi_{i+1,j+1}-\varphi_{i,j+1}}{h} - \dfrac{\varphi_{i+1,j}-\varphi_{i,j}}{h}}{h}\right)h^2. \tag{14}$$

Thus, the topological charge at the phase singularity is $\rho = \pm 1$, and 0 elsewhere.[46]

3. Results

3.1. Direct current electric fields

To reveal the effect of a direct current electric field on the drift behavior of counter-rotating spiral waves, we consider two cases: a direct current electric field along the y direction and along the $-y$ direction. Figure 1 illustrates the constant electric field-induced drift of spiral waves in different directions, where the yellow curves in Figs. 1(c) and 1(f) denote the trajectories of counterclockwise spiral waves, the blue curves denote the trajectories of clockwise spiral waves, and the arrows indicate the drift directions of the spiral waves.

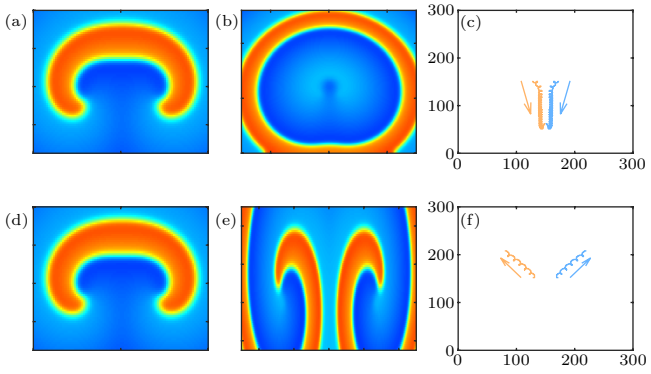


Fig. 1. Drift of counter-rotating spiral waves induced by a direct current electric field. Electric fields applied in opposite directions drive the two spiral waves to drift along different paths. The yellow curve denotes the trajectory of the counterclockwise spiral wave, and the blue curve denotes that of the clockwise spiral wave. Direct current electric field applied along the $-y$ direction with magnitude $E_0 = 0.32$: (a) $t = 0$; (b) $t = 204$; (c) tip trajectories. Direct current electric field applied along the $+y$ direction with the same magnitude $E_0 = 0.32$: (d) $t = 0$; (e) $t = 70$; (f) tip trajectories.

We set the x-component of the electric field to $E_x = 0$ and consider only a constant electric field along a single direction. When an electric field along the $-y$ direction is applied, as shown in Figs. 1(a)–1(c). Figure 1(a) shows the initial state with a counterclockwise spiral on the left and a clockwise spiral on the right. After a period of evolution, the two spiral waves gradually approach each other and eventually undergo annihilation, as shown in Fig. 1(b). Figure 1(c) illustrates the drift trajectories: the spirals are initially attracted to each other, and when their spacing narrows to a certain critical value, the two tips drift downward along the electric field direction and subsequently meet and annihilate.

Conversely, when a direct current electric field along the y direction is applied, as shown in Figs. 1(d)–1(f), Fig. 1(d) shows the initial state, which is identical to Fig. 1(a), and the two spiral waves gradually move away from each other over time (Fig. 1(e)). Figure 1(f) shows the corresponding tip drift trajectories, with the two spirals drifting toward the left and right boundaries, respectively, indicating a tendency to move apart.

In the initial stages of Figs. 1(c) and 1(f), the yellow arrows are antiparallel, as are the blue arrows, indicating that spirals with the same chirality drift in opposite directions when the electric field is reversed. As evolution proceeds, in Fig. 1(c) the distance between the two spiral tips gradually decreases, and the spirals enter the short-range attraction range, causing their drift trajectories to deviate from the original directions. In contrast, in Fig. 1(f), the distance between the spiral tips increases, there is almost no interaction, and the drift directions remain essentially unchanged. Thus, the arrows are not exactly antiparallel, reflecting the influence of spiral interactions on the drift.

The drift behavior of spiral tips under an electric field is affected by the combined influence of rotation direction and electric field direction. For counter-rotating spirals, they exhibit a transverse drift component opposite to the electric field. If the field induces the spirals to approach each other, as shown in Figs. 1(a)–1(c), they enter the short-range attraction regime when their horizontal distance falls below 20, resulting in annihilation. If the field drives the spirals apart, as shown in

Figs. 1(d)–1(f), they remain separated.

In conclusion, under a direct current electric field, spiral waves exhibit a transverse drift component perpendicular to the field direction, in addition to drifting along the field. The direction of this transverse drift depends on both the electric field and the rotation direction of the spiral waves, being opposite for counter-rotating spirals. Thus, the electric field can either bring spirals together to annihilate them, as shown in Figs. 1(a)–1(c), or drive them apart, as shown in Figs. 1(d)–1(f). This annihilation behavior results from the combination of field-induced trajectory reorientation and the short-range attraction mechanism between spirals.

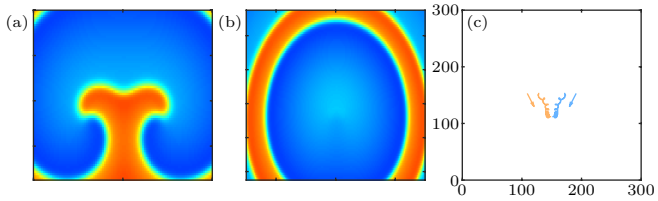


Fig. 2. The wavelength of the spiral waves affects the critical distance at which they become mutually attractive. The yellow curve shows the trajectory of a counterclockwise spiral wave, and the blue curve shows the trajectory of a clockwise spiral wave. The direct current electric field is applied along the $-y$ direction with an electric field intensity of $E_0 = 0.32$ and $D = 0.9$. (a) $t = 0$; (b) $t = 80$; (c) tip trajectories.

The wavelength of the spiral waves in Fig. 1(a) is 0.1818. To investigate the effect of wavelength on the drift behavior of spiral waves, we adjusted the diffusion coefficient D to 0.9 to obtain new spiral waves with a wavelength of 0.1653. A direct current electric field with intensity $E_0 = 0.32$ is then applied in the $-y$ direction. Figure 2(a) shows the initial state of the spiral waves, where the initial distance between the two spiral tips is 44, consistent with the case in Fig. 1(a). After a period of evolution, the spiral waves begin to attract each other and eventually undergo annihilation, as shown in Fig. 2(b). The drift trajectory of the spiral waves is illustrated in Fig. 2(c). Measurements indicate that the horizontal distance between the two spiral tips is about 20 when attraction begins under the conditions shown in Fig. 1(c), whereas in Fig. 2(c), it is only 12 when attraction occurs. This result demonstrates that the critical distance required for mutual attraction of spiral waves is closely related to their wavelength: the shorter the wavelength, the smaller the critical distance.

It has been shown that the annihilation of a spiral wave usually occurs between a pair of counter-rotating spiral waves. When they are close enough, the spirals are connected by an activation front, forming a propagation channel. If this channel is blocked by the polarization region, the activation front contracts rapidly, leading to the simultaneous disappearance of the entire pair of spiral tips, i.e., annihilation occurs.[56] In this process, there is an apparent short-range attractive interaction between the spiral waves, and the range of this interaction decreases with decreasing wavelength. A smaller spiral structure corresponds to a smaller effective radius of action, meaning that only at closer distances is the interaction strong enough to trigger annihilation. Thus, the shorter the wavelength, the smaller the critical proximity distance required for annihilation, resulting in a higher likelihood of close interaction at a lower critical distance.

3.2. Alternating current electric fields

Unless otherwise stated, the initial state of the spiral waves is as shown in Fig. 1(a). We set the coordinates of the center of the left spiral wave to (130, 152) and the center of the right spiral wave to (170, 152), and establish a polar reference system with the horizontal direction as the polar axis. The initial phase angle of the left spiral wave is π, and that of the right spiral wave is zero. The period of rotation of the spiral waves is 11.0171, and the wavelength is 0.1818.

To study the effect of an alternating current electric field on counter-rotating spiral waves, we simulate the evolution of spiral waves with opposite chirality under alternating current electric fields with different phase angles, as shown in Fig. 3. The alternating current electric field is given by $E_y = E_0 \cos(\omega t + \phi_0)$, where ϕ_0 is the phase angle. Here, we set $\omega = 2\omega_{\text{spiral}}$ and the field intensity to $E_0 = 0.13$. In the figure, the yellow curve indicates the trajectory of the counterclockwise spiral wave, and the blue curve indicates the trajectory of the clockwise spiral wave.

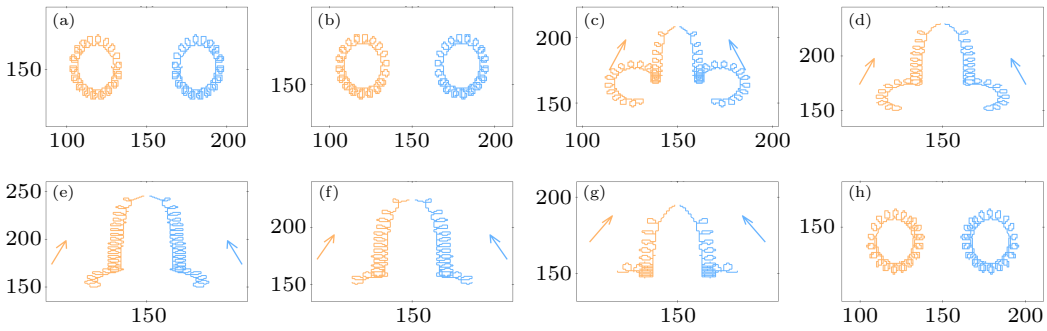


Fig. 3. Effect of different modes of alternating current electric fields on the annihilation of counter-rotating spiral waves. The spiral waves annihilate differently under the control of alternating current electric fields with different initial phases. The phases of the alternating current electric field are (a) $\phi_0 = 0$, (b) $\phi_0 = \pi/4$, (c) $\phi_0 = \pi/2$, (d) $\phi_0 = 3\pi/4$, (e) $\phi_0 = \pi$, (f) $\phi_0 = 5\pi/4$, (g) $\phi_0 = 3\pi/2$, (h) $\phi_0 = 7\pi/4$. The electric field is given by $E_y = E_0 \cos(\omega t + \phi_0)$, $E_x = 0$, with $E_0 = 0.13$ and $\omega = 2\omega_{\text{spiral}}$.

When the phase angle ϕ_0 is 0, $\pi/4$, or $7\pi/4$, the simulation results are shown in Figs. 3(a), 3(b), and 3(h), where the two spiral waves rotate within a small range of trajectories near their respective initial positions and fail to undergo annihilation. Although the initial states and the timing of the electric field application are identical, differences in phase angles lead to variations in the initial drift directions of the spiral waves, resulting in trajectories that are roughly similar but differ in specific paths, ultimately failing to reach the critical distances required for interaction.

When $\phi_0 = \frac{\pi}{2}$, as shown in Fig. 3(c), the two spiral waves initially approach each other gradually along arc-shaped trajectories, reaching a critical distance during the downward drift, and then drift upward together, eventually undergoing mutual attraction and annihilation. As the phase angle increases to $\phi_0 = \frac{3\pi}{4}$ and $\phi_0 = \pi$ (Figs. 3(d) and 3(e)), the curvature of the arc trajectories gradually decreases and the upward drift distance increases, indicating that the spiral waves can still complete the attraction and annihilation process at longer distances. Further increasing the phase angle to $\phi_0 = \frac{5\pi}{4}$ and $\phi_0 = \frac{3\pi}{2}$ (Figs. 3(f) and 3(g)), the trajectories continue to shrink and the upward drift gradually decreases. Thus, the phase angle affects not only the drift directions but also the drift distances of the spiral waves.

In summary, the phase angle of the alternating current electric field has a significant effect on the interaction and annihilation behavior of counter-rotating spiral waves. Mutual attraction and annihilation occur only when the spiral tips reach a certain spatial proximity during their trajectory evolution. This attraction originates from the short-range interaction between the spiral waves. When the two counter-rotating spiral tips approach each other and the electric field drives them into the short-range interaction zone, the activation front can be blocked by the polarization region, forming a wave block that triggers contraction of the activation front, ultimately leading to the simultaneous disappearance of the two spiral tips, i.e., annihilation. This process requires a high degree of proximity between the tips, so that annihilation occurs only when the electric field induces drift trajectories favorable for approximation, as in Figs. 3(c)–3(g). In contrast, under other phase conditions (Figs. 3(a), 3(b), and 3(h)), the spiral waves are unlikely to annihilate because they fail to approach each other sufficiently.

We use three statistics — the average membrane potential (u_{mean}), the order parameter (A), and the synchronization error (E) — as indicators of spiral wave annihilation, to further quantify the impact of phase angle on counter-rotating spiral waves. Figure 4 illustrates the trends of these three statistics with phase ϕ_0. Arrow labels indicate the ranges where the statistics drop significantly. The total simulation time is set to 500, and the range 400–500 is used for calculation.

Figure 4(a) shows the trend of u_{mean} with phase angle. The average membrane potential decreases significantly when the phase angle varies from $\frac{19\pi}{40}$ to $\frac{81\pi}{51}$, suggesting that within this phase range, two spiral waves of opposite chirality can undergo mutual annihilation, reducing the overall activity of the system. Figure 4(b) shows the variation of the order parameter A, which also decreases significantly in the same phase range, indicating strong modulation of spiral wave annihilation by the phase angle. The synchronization error E, shown in Fig. 4(c), further confirms this observation: E drops to 0 in this phase range, indicating that no node in the network is excited and the spiral waves have annihilated.

In summary, two spiral waves of opposite chirality can annihilate each other under specific phase angle conditions, leading to a significant decrease in u_{mean}, A, and E. This result suggests that the phase angle of the electric field modulates the spiral wave drift directions, and only under specific phase conditions do the spiral tips enter the short-range attraction interaction zone, allowing significant interaction, upward motion together, and eventual mutual annihilation. Spiral wave annihilation relies on the overlap and proximity of the tip trajectories, modulated by the electric field phase angle; only when the tips are sufficiently close and an activation front connection is formed can a short-range attraction occur, leading to final annihilation.

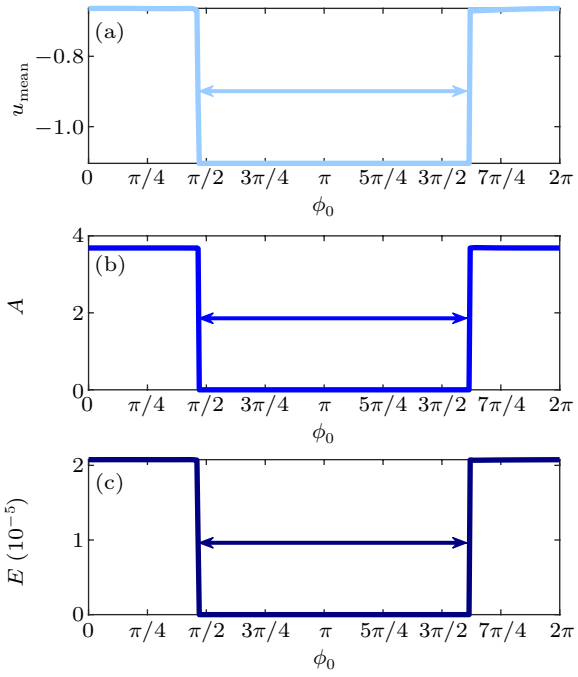


Fig. 4. Annihilation of counter-rotating spiral waves occurs only under specific phase conditions. (a) u_{mean}, (b) A, and (c) E as functions of the phase ϕ_0. Bidirectional arrows indicate the ranges where abrupt drops occur.

In order to further reveal the modulating effect of the electric field intensity E_0 on the interaction of spiral waves, we investigated the variation of three statistics with E_0. Figure 5 illustrates the trends of these statistics as a function of E_0, where

the initial phase of the alternating current electric field is set to $\phi_0 = \pi$.

As the electric field intensity gradually increases and reaches the critical value $E_0 = 0.13$, the average membrane potential u_{mean} exhibits a sudden and pronounced drop, as shown in Fig. 5(a). This indicates that the electric field can drive interaction and annihilation of the spiral waves along their upward drift only when the intensity exceeds a threshold. Figure 5(b) shows the variation of A with E_0, which also decreases sharply at the same critical point, indicating that the excitability of the spiral waves is significantly weakened. Similarly, the synchronization error E, shown in Fig. 5(c), drops abruptly at this critical value, further confirming that the spiral waves undergo annihilation.

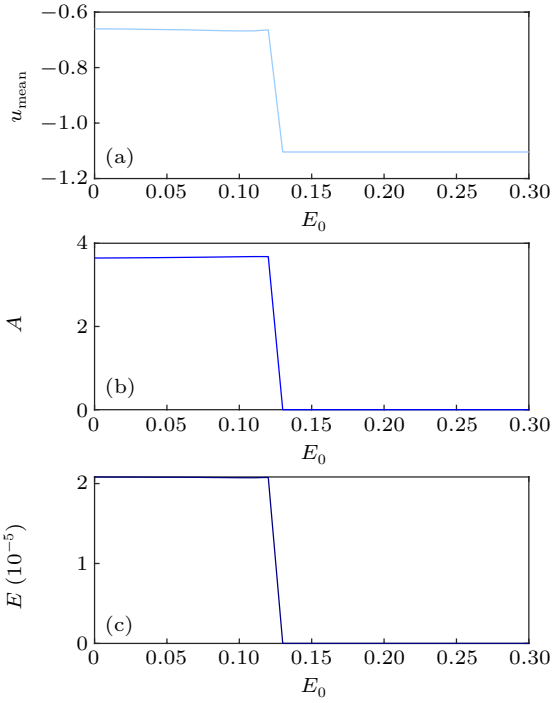


Fig. 5. Annihilation of the counter-rotating spiral waves occurs only when the electric field intensity E_0 is increased beyond a certain threshold. Variation of (a) u_{mean}, (b) A, and (c) E with the electric field intensity E_0.

The annihilation of spiral waves depends on whether the two spiral tips can enter the short-range attraction range during their motion. When the intensity of the electric field is weak ($E_0 < 0.13$), although the tips drift periodically, the minimum proximity distance between them remains larger than the critical distance required to trigger attraction. As a result, no activation front connection can be formed, and annihilation does not occur. When E_0 exceeds a certain threshold, the drift drive of the electric field on the spiral tips is significantly enhanced, allowing them to approach closely enough to enter the effective attraction range. At this point, if the activation front is spatially connected and blocked by an electric field or polarization region, wave blocking may occur, triggering activation front collapse and ultimately leading to synchronous annihilation of the tips.

In summary, only when the electric field intensity E_0 reaches a particular threshold can the two spiral waves approach sufficiently close during their motion to interact significantly. This interaction drives the two spiral tips into a synergistic drift that eventually results in mutual annihilation.

We further investigated the case of an alternating current electric field applied in the x-direction, given by $E_{x\text{L}} = E_0\cos(\omega t + \phi)$, $E_{x\text{R}} = -E_0\cos(\omega t + \phi)$, where ϕ is the phase angle, the frequency is set to $\omega = 2\omega_{\text{spiral}}$, and the intensity of the electric field is $E_0 = 0.15$. Figure 6 demonstrates the interaction process of two spiral waves at different phase angles. The yellow curve indicates the trajectory of the counterclockwise spiral wave, and the blue curve indicates the trajectory of the clockwise spiral wave.

When the phase angle $\phi = 0$, as shown in Fig. 6(a), the two spiral waves initially approach each other along an arc trajectory and reach the critical distance required for interaction during drift, followed by drift in the same direction and eventual annihilation. As the phase angle increases gradually to $\phi = \frac{\pi}{4}$ up to π (Figs. 6(b)–6(e)), the two spiral waves rotate near their respective initial positions without mutual annihilation. This behavior is mainly due to the initial drift directions of the two spiral waves not coinciding under different phase conditions, preventing them from reaching the distance required for effective interaction and annihilation.

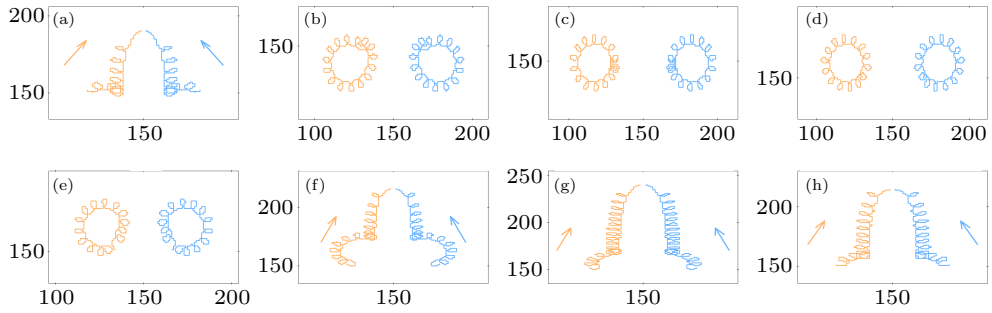


Fig. 6. The effect of different modes of alternating current electric fields on the annihilation of counter-rotating spiral waves. The yellow curve shows the trajectory of the counterclockwise spiral wave, and the blue curve shows the trajectory of the clockwise spiral wave. Different modes of alternating current electric fields lead to different annihilation behaviors. The phases of the alternating current electric field are (a) $\phi = 0$, (b) $\phi = \pi/4$, (c) $\phi = \pi/2$, (d) $\phi = 3\pi/4$, (e) $\phi = \pi$, (f) $\phi = 5\pi/4$, (g) $\phi = 3\pi/2$, (h) $\phi = 7\pi/4$. The applied field is $E_{x\text{L}} = E_0\cos(\omega t + \phi)$, $E_{x\text{R}} = -E_0\cos(\omega t + \phi)$, $E_y = 0$, with $E_0 = 0.15$ and $\omega = 2\omega_{\text{spiral}}$.

When the phase angle is increased to $\phi = \frac{5\pi}{4}$, as shown in Fig. 6(f), the trajectories of the two spiral waves change significantly compared to Fig. 6(a), with the arc-shaped trajectories notably enlarged, indicating a significant shift in the initial drift direction. Further increasing the phase angle to $\phi = \frac{3\pi}{2}$ (Fig. 6(g)) and $\phi = \frac{7\pi}{4}$ (Fig. 6(h)), the arc drifts of the two spiral waves are weakened, but the upward drift trajectories increase and move almost along parallel straight lines. This indicates that although mutual annihilation can still occur under these phase conditions, the interaction is weaker and the time required for annihilation is longer.

When a suitable phase angle is chosen, the two counter-rotating tips drift close together under the drive of an electric field and approach a critical distance, thereby entering the short-range attraction range, which triggers annihilation. In contrast, when the electric field phase is improperly set, resulting in a large difference in the drift directions of the two spiral wave tips, their trajectories cannot effectively converge, and the tip spacing remains larger than the critical attraction distance. This prevents the formation of an activation front connection, and annihilation cannot occur.

In summary, the phase angle ϕ is an important parameter for modulating spiral wave interactions. Under the action of an alternating current electric field, specific phase conditions can induce synchronized drift and interaction of two spiral waves at suitable locations and time scales, which in turn leads to annihilation. Conversely, inappropriate phase settings can cause differences in the drift directions of the spiral waves, preventing effective approach and thus annihilation.

Whether annihilation of counter-rotating spiral waves occurs depends not only on the parameters of the alternating current electric field but also on the initial phase combination of the spiral waves. The initial phase angles of the left and right spiral wave tips can be obtained by calculating the direction angle of the tip, $\theta_i = \tan^{-1}(\mathrm{d}y/\mathrm{d}x)$. The response behavior of the spiral waves under different initial phase combinations is further extracted by recording tip positions at different time points. Figures 7(a)–7(h) illustrate the effect of different initial phase combinations on annihilation behavior under a longitudinal alternating current electric field, $E_x = 0$, $E_y = E_0\cos(\omega t + \phi_0)$, with $\phi_0 = \pi$ and $E_0 = 0.13$. When the initial phases are $\theta_1 = \pi$, $\theta_2 = 0$ (Fig. 7(a)), $\theta_1 = \frac{5\pi}{4}$, $\theta_2 = \frac{7\pi}{4}$ (Fig. 7(b)), $\theta_1 = 0$, $\theta_2 = \pi$ (Fig. 7(e)), $\theta_1 = \frac{\pi}{4}$, $\theta_2 = \frac{3\pi}{4}$ (Fig. 7(f)), and $\theta_1 = \frac{3\pi}{4}$, $\theta_2 = \frac{\pi}{4}$ (Fig. 7(h)), the counter-rotating spiral waves successfully undergo mutual annihilation. In contrast, when the initial phases are $\theta_1 = \frac{3\pi}{2}$, $\theta_2 = \frac{3\pi}{2}$ (Fig. 7(c)), $\theta_1 = \frac{7\pi}{4}$, $\theta_2 = \frac{5\pi}{4}$ (Fig. 7(d)), or $\theta_1 = \frac{\pi}{2}$, $\theta_2 = \frac{\pi}{2}$ (Fig. 7(g)), the spiral waves fail to stabilize their approach and do not undergo annihilation.

The effect of the initial phase on spiral wave evolution is further demonstrated in Figs. 7(i)–7(p) under a transverse alternating current electric field, $E_{x\mathrm{L}} = E_0\cos(\omega t + \phi)$, $E_{x\mathrm{R}} = E_0\cos(\omega t + \phi)$, $E_y = 0$, $\phi = 0$, $E_0 = 0.15$. Annihilation occurs when the initial phases are $\theta_1 = \pi$, $\theta_2 = 0$ (Fig. 7(i)), $\theta_1 = \frac{5\pi}{4}$, $\theta_2 = \frac{7\pi}{4}$ (Fig. 7(j)), $\theta_1 = \frac{3\pi}{2}$, $\theta_2 = \frac{3\pi}{2}$ (Fig. 7(k)), $\theta_1 = \frac{\pi}{4}$, $\theta_2 = \frac{3\pi}{4}$ (Fig. 7(n)), and $\theta_1 = \frac{\pi}{2}$, $\theta_2 = \frac{\pi}{2}$ (Fig. 7(o)). However, initial phase combinations of $\theta_1 = \frac{7\pi}{4}$, $\theta_2 = \frac{5\pi}{4}$ (Fig. 7(l)), $\theta_1 = 0$, $\theta_2 = \pi$ (Fig. 7(m)), or $\theta_1 = \frac{3\pi}{4}$, $\theta_2 = \frac{\pi}{4}$ (Fig. 7(p)) fail to produce effective contact and annihilation.

Essentially, whether spiral waves undergo annihilation depends on whether two antichiral spiral waves can achieve effective spatial proximity under the influence of an electric field. Differences in initial phase can significantly alter the initial drift directions, determining whether the tips can progressively approach along a favorable path. If, during motion,

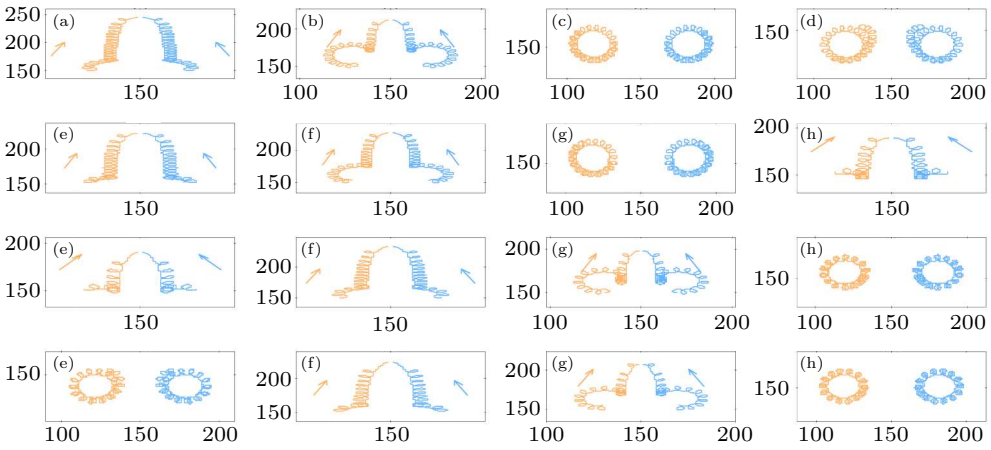


Fig. 7. Effect of the alternating current electric field on the annihilation of reverse-rotating spiral waves at different initial states. The initial phase combinations of the spiral waves are (a) $\theta_1 = \pi$, $\theta_2 = 0$, (b) $\theta_1 = \frac{5\pi}{4}$, $\theta_2 = \frac{7\pi}{4}$, (c) $\theta_1 = \frac{3\pi}{2}$, $\theta_2 = \frac{3\pi}{2}$, (d) $\theta_1 = \frac{7\pi}{4}$, $\theta_2 = \frac{5\pi}{4}$, (e) $\theta_1 = 0$, $\theta_2 = \pi$, (f) $\theta_1 = \frac{\pi}{4}$, $\theta_2 = \frac{3\pi}{4}$, (g) $\theta_1 = \frac{\pi}{2}$, $\theta_2 = \frac{\pi}{2}$, (h) $\theta_1 = \frac{3\pi}{4}$, $\theta_2 = \frac{\pi}{4}$, (i) $\theta_1 = \pi$, $\theta_2 = 0$, (j) $\theta_1 = \frac{5\pi}{4}$, $\theta_2 = \frac{7\pi}{4}$, (k) $\theta_1 = \frac{3\pi}{2}$, $\theta_2 = \frac{3\pi}{2}$, (l) $\theta_1 = \frac{7\pi}{4}$, $\theta_2 = \frac{5\pi}{4}$, (m) $\theta_1 = 0$, $\theta_2 = \pi$, (n) $\theta_1 = \frac{\pi}{4}$, $\theta_2 = \frac{3\pi}{4}$, (o) $\theta_1 = \frac{\pi}{2}$, $\theta_2 = \frac{\pi}{2}$, (p) $\theta_1 = \frac{3\pi}{4}$, $\theta_2 = \frac{\pi}{4}$. Here, θ_1 and θ_2 denote the initial phases of the left and right spiral tips, respectively. The longitudinal alternating current electric field is applied in (a)–(h): $E_x = 0$, $E_y = E_0\cos(\omega t + \phi_0)$, $\phi_0 = \pi$, $E_0 = 0.13$. The transverse alternating current electric field is applied in (i)–(p): $E_{x\mathrm{L}} = E_0\cos(\omega t + \phi)$, $E_{x\mathrm{R}} = E_0\cos(\omega t + \phi)$, $E_y = 0$, $\phi = 0$, $E_0 = 0.15$, $\omega = 2\omega_{\mathrm{spiral}}$.

the tips enter the interaction range, i.e., within the critical attraction distance, and the activation fronts are spatially connected while simultaneously influenced by an external electric field or a localized blocking region, the instability of the activation fronts may be triggered, leading to their disintegration and ultimately to the synchronous annihilation of the two tips. Conversely, if the initial phase combination produces large angular deviations or spatial separations between the drift trajectories, the tips cannot approach sufficiently close, the interactions remain weak, and activation fronts cannot connect, preventing annihilation.

In summary, the interaction between spiral waves is not only highly sensitive to the frequency and intensity of the electric field, but also strongly dependent on the combination of initial phase angles. A reasonable choice of the initial phase can modulate the relative motion tendencies of the spiral waves, thereby determining whether mutual annihilation occurs.

3.3. Polarized electric fields

In this section, we investigate the role of polarized electric fields in modulating the annihilation process of counter-rotating spiral waves. Different origins are chosen for the left and right spiral waves, with the left spiral wave at (130, 152) and the right spiral wave at (170, 152).

The kinetic behavior of the spiral waves is systematically investigated by varying the phase, intensity, and angular frequency of the polarized electric field, as well as the initial phase of the spiral waves. The polarized electric field can be expressed as a combination of three components: $E_{x\mathrm{L}} = E_0\cos(\omega t + \phi_1)$, $E_{x\mathrm{R}} = -E_0\cos(\omega t + \phi_1)$, $E_y = E_0\cos(\omega t + \phi_2)$, where ϕ_1 and ϕ_2 are the initial phases in the x and y directions, respectively. Different phase combinations significantly affect the trajectories of the two spiral tips and their interaction processes.

Figure 8 demonstrates the modulating effect of the polarized electric field on the annihilation behavior of counter-rotating spiral waves for various phase configurations. It can be seen that the spiral waves can achieve mutual annihilation under the action of an applied polarized electric field for all selected phase combinations. Nonetheless, the drift trajectories of the two spiral tips differ greatly in shape and angle across the different phase combinations, with notable variations in initial drift direction and curvature.

For example, when the phase combinations are $(0, \pi)$ (Fig. 8(a)) and $\left(\frac{3\pi}{2}, \frac{3\pi}{2}\right)$ (Fig. 8(f)), the two trajectories are almost identical, with the spiral waves first bending upward to approach each other, followed by drifting in the same direction and ultimately achieving annihilation. Similarly, for phase combinations $\left(\frac{\pi}{4}, \frac{5\pi}{4}\right)$ (Fig. 8(b)) and $\left(\frac{7\pi}{4}, \frac{7\pi}{4}\right)$ (Fig. 8(h)), the trajectories remain highly similar. The circular trajectories of both spiral waves are larger and closely matched for (π, π) (Fig. 8(c)) and $\left(\frac{3\pi}{2}, \frac{\pi}{2}\right)$ (Fig. 8(e)), as well as for $\left(\frac{5\pi}{4}, \frac{5\pi}{4}\right)$ (Fig. 8(d)) and $\left(\frac{7\pi}{4}, \frac{3\pi}{4}\right)$ (Fig. 8(g)).

The mechanism behind this trajectory similarity can be attributed to the combination of phases in both directions of the polarized electric field. A relative difference in the phases (ϕ_1, ϕ_2) along the two directions can change the direction and amplitude of the resulting electric field, which in turn affects the actual drift trajectory of the spiral waves. When the polarized electric field has different phase combinations in the two directions, the direction of the combined force changes periodically with time, causing the spiral waves to bend or shift differently during drift. The drift trajectories in Figs. 8(a) and 8(f), 8(b) and 8(h), 8(c) and 8(e), and 8(d) and 8(g) show a high degree of consistency. Further analysis reveals that, in cases where trajectories are similar, the difference $\left|(\phi_{1i} + \phi_{2i}) - (\phi_{1j} + \phi_{2j})\right|$ between the sums of the corresponding initial phases is constant, where i and j denote the image indices (a)–(h), respectively.

Further, to more clearly reveal the effects of different phase combinations on the drift behavior of spiral waves, we quantitatively analyze their drift trajectories. The trajectories of the spiral tips show significant differences under different phase conditions, particularly in the maximum offset angle

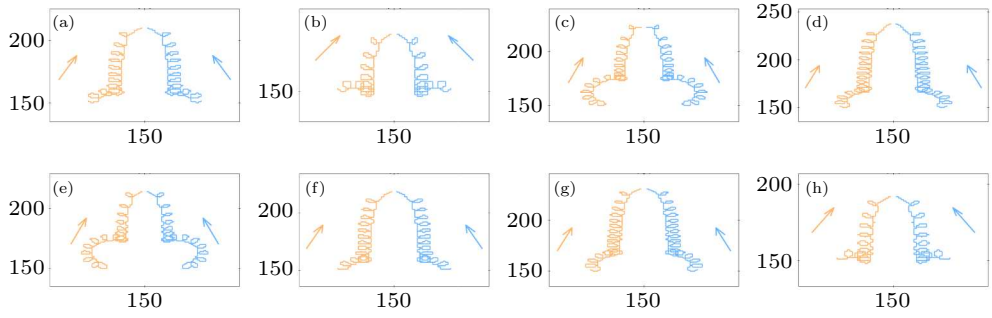


Fig. 8. The yellow curve shows the trajectory of the counterclockwise spiral wave, while the blue curve shows the trajectory of the clockwise spiral wave. These plots illustrate the effects of different polarized electric field modes on the annihilation of counter-rotating spiral waves. The phases of the polarized electric field are (a) $\phi_1 = 0$, $\phi_2 = \pi$, (b) $\phi_1 = \pi/4$, $\phi_2 = 5\pi/4$, (c) $\phi_1 = \pi$, $\phi_2 = \pi$, (d) $\phi_1 = 5\pi/4$, $\phi_2 = 5\pi/4$, (e) $\phi_1 = 3\pi/2$, $\phi_2 = \pi/2$, (f) $\phi_1 = 3\pi/2$, $\phi_2 = 3\pi/2$, (g) $\phi_1 = 7\pi/4$, $\phi_2 = 3\pi/4$, (h) $\phi_1 = 7\pi/4$, $\phi_2 = 7\pi/4$. The electric field components are given by $E_{x\mathrm{L}} = E_0\cos(\omega t + \phi_1)$, $E_{x\mathrm{R}} = -E_0\cos(\omega t + \phi_1)$, $E_y = E_0\cos(\omega t + \phi_2)$, with $E_0 = 0.1$ and $\omega = 2\omega_{\mathrm{spiral}}$.

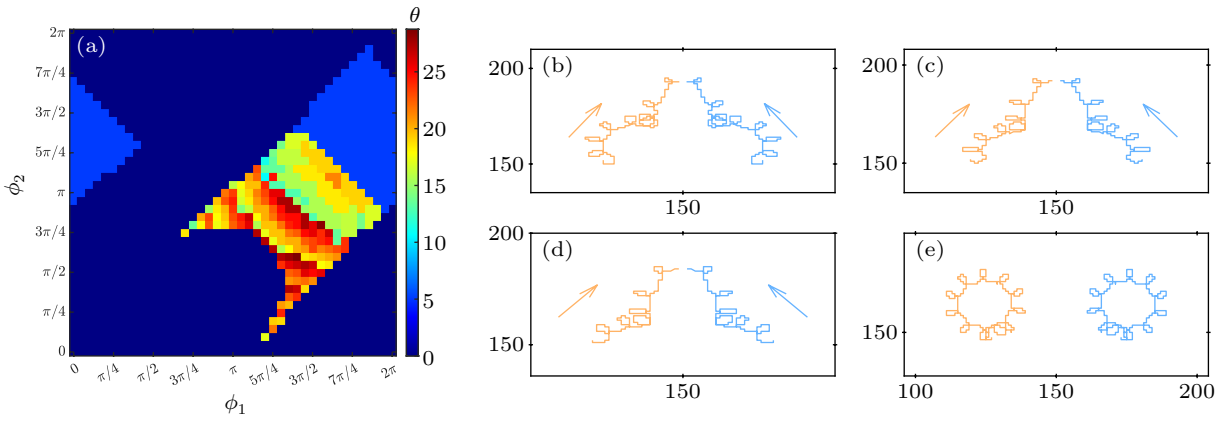


Fig. 9. Different maximum offset angles of spiral waves induced by various polarized electric fields. (a) The horizontal axis represents the phase of the polarized electric field in the x-direction, and the vertical axis represents the phase of the polarized electric field in the y-direction. The different colors indicate different offset angles of the spiral waves; if the two spiral waves do not annihilate, the offset angle is taken to be 0. On the right are the plots of the trajectories corresponding to different offset angles, with phase combinations: (b) $\phi_1 = 7\pi/5$, $\phi_2 = 9\pi/10$, (c) $\phi_1 = 8\pi/5$, $\phi_2 = \pi$, (d) $\phi_1 = 9\pi/5$, $\phi_2 = 6\pi/5$, (e) $\phi_1 = \pi$, $\phi_2 = \pi/2$. The electric field components are given by $E_{x\mathrm{L}} = E_0\cos(\omega t + \phi_1)$, $E_{x\mathrm{R}} = -E_0\cos(\omega t + \phi_1)$, $E_y = E_0\cos(\omega t + \phi_2)$, with $E_0 = 0.1$ and $\omega = 2\omega_{\mathrm{spiral}}$.

and trajectory displacement. The variation of the maximum offset angle θ for different phase combinations is visualized in Fig. 9, and Fig. 10 shows the general trend of the trajectory displacement with respect to the phase combinations.

Using the point (151, 150) as the origin, a polar coordinate system is established with the vertical direction upward and the horizontal direction to the right. The polar angle corresponding to the point with the largest horizontal displacement of the right-side spiral wave is defined as the maximum offset angle θ. This offset angle is recorded as zero if the spiral waves do not undergo annihilation.

Figure 10(a) illustrates the distribution of θ with respect to the phase combination (ϕ_1, ϕ_2), where the red region indicates a larger maximum offset angle and the blue region indicates a smaller angle. The distribution exhibits a clear band structure, suggesting that the amplitude of the offset angle is relatively similar when $\left|(\phi_{1i} + \phi_{2i}) - (\phi_{1j} + \phi_{2j})\right|$ is constant.

This demonstrates a correlation between the magnitude of the offset angle and the sum of the two phases $\phi_1 + \phi_2$. This correlation arises because the drift direction of the spiral waves is influenced not only by the relative phase between the two electric fields but also by the initial synthesized direction and magnitude of the electric field. In other words, $\phi_1 + \phi_2$ affects the phase of the initial synthesized electric field, thereby altering the overall offset trend of the spiral wave trajectory.

Specifically, $\phi_1 = 7\pi/5$, $\phi_2 = 9\pi/10$ in Fig. 9(b), corresponding to the red region of the color map, indicates a large offset angle. Figure 9(c) with $\phi_1 = 8\pi/5$, $\phi_2 = \pi$ corresponds to the green region. Figure 9(d) with $\phi_1 = 9\pi/5$, $\phi_2 = 6\pi/5$ corresponds to the bright blue region. Figure 9(e) with $\phi_1 = \pi$, $\phi_2 = \pi/2$ corresponds to the dark blue region, indicating that annihilation did not occur.

Therefore, the significant differences in maximum offset angles reflect the strong modulation of phase combinations on spiral wave drift behavior. The initial phase combination (ϕ_1, ϕ_2) in both directions of the electric field determines the direction and amplitude of the synthesized electric field. When $\left|(\phi_{1i} + \phi_{2i}) - (\phi_{1j} + \phi_{2j})\right|$ is constant, the two spiral waves experience similar combined electric forces, and their drift trajectories show similar trends, making it easier for them to approach each other along comparable paths and interact, or even annihilate. Conversely, if the phase combination produces a large difference in drift directions between the two spiral waves, the trajectory folding angle decreases or becomes opposed, preventing the tips from approaching sufficiently. In such cases, no activation front connection is formed, and annihilation cannot occur. This also explains the banding of red regions (large offset angle) with blue regions (small offset angle) in Fig. 9(a), indicating that the system is highly selective with respect to phase combinations.

In summary, different phase combinations significantly affect the maximum offset angle of the spiral waves, with the variation of the phase sum $\phi_1 + \phi_2$ playing a key role in modulating the offset behavior. A reasonable combination of phases increases the likelihood that two spiral waves will approach each other and annihilate, whereas inappropriate phase combinations can lead to large differences in drift direction and ultimately prevent annihilation.

Figure 10 illustrates the variation in trajectory displacements of spiral waves undergoing mutual annihilation for different combinations of polarized electric field phases (ϕ_1, ϕ_2). If the two spiral waves do not annihilate, the trajectory displacement is taken to be zero. In Fig. 10(a), the horizontal coordinate represents the phase ϕ_1 in the x-direction, and the vertical coordinate represents the phase ϕ_2 in the y-direction. Different colors indicate the magnitude of trajectory displacement during spiral wave annihilation, with warmer colors representing larger displacements.

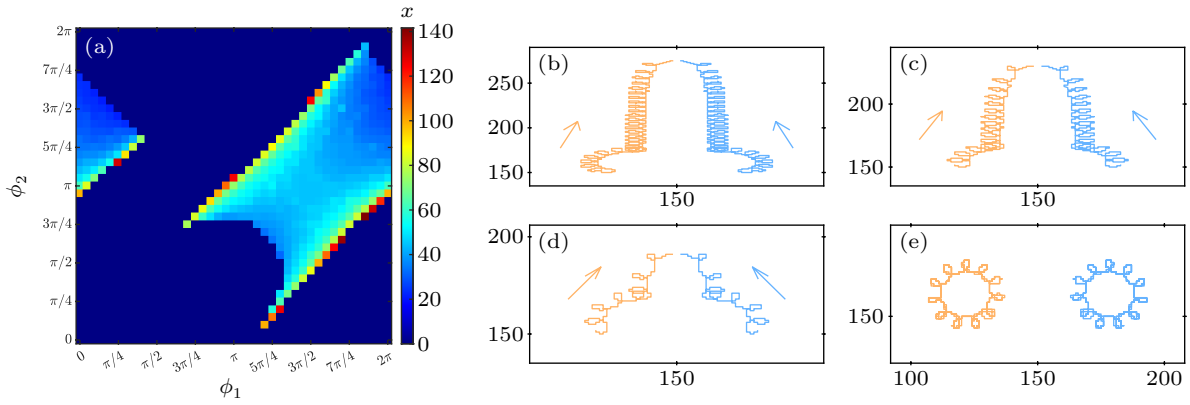


Fig. 10. Different displacements of spiral wave trajectories induced by various polarized electric fields. (a) The horizontal axis represents the phase in the x-direction of the polarized electric field, and the vertical axis represents the phase in the y-direction. Different colors indicate different trajectory displacements of the spiral waves. If the two spiral waves do not annihilate, the trajectory displacement is assumed to be zero. On the right are the trajectory maps corresponding to different trajectory displacements, with phase combinations: (b) $\phi_1 = \pi$, $\phi_2 = 21\pi/20$, (c) $\phi_1 = 9\pi/5$, $\phi_2 = 4\pi/5$, (d) $\phi_1 = 3\pi/2$, $\phi_2 = \pi$, (e) $\phi_1 = 3\pi/4$, $\phi_2 = \pi/2$. The electric field components are given by $E_{\mathrm{xL}} = E_0\cos(\omega t + \phi_1)$, $E_{\mathrm{xR}} = -E_0\cos(\omega t + \phi_1)$, $E_y = E_0\cos(\omega t + \phi_2)$, with $E_0 = 0.1$ and $\omega = 2\omega_{\mathrm{spiral}}$.

The figure shows that the trajectory displacements exhibit a clear banding structure in the parameter space. The displacement is most pronounced when the phase difference between ϕ_1 and ϕ_2 is close to 0 or π. This suggests that under these phase conditions, spiral waves experience a more significant overall drift due to the driving effect before sufficiently strong interactions occur. This enhanced trajectory migration arises because the linearly polarized electric field maintains a relatively stable driving direction, continuously guiding both spiral waves to drift in the same direction. Corresponding to Figs. 10(b) and 10(c), the two spiral waves move significantly along the perpendicular direction and eventually undergo annihilation.

In contrast, under a nonlinearly polarized electric field, the spiral waves exhibit more complex dynamical behavior. As shown in Figs. 10(d) and 10(e), the electric field direction varies periodically in time, resulting in more complex rotational actuation. In Fig. 10(d), the migration speed is accelerated but the drift distance is shorter, suggesting that the periodic change in the field's rotation direction enhances localized interactions between the spiral waves, thereby accelerating annihilation. This indicates that in a polarized electric field, variability in the field direction promotes stronger localized action rather than maintaining a persistent drift path, leading to more efficient but less displaced annihilation. Figure 10(e) illustrates another typical nonlinear polarization scenario, where the failure of the spiral waves to annihilate indicates that this phase combination does not bring the waves within the interaction distance required for annihilation.

In summary, in a nonlinearly polarized electric field, the drift trajectory of spiral waves is determined not only by the local driving direction but also synergistically by the combination of phases in both directions of the electric field. A proper phase combination can steadily guide the spiral waves toward each other, resulting in annihilation, whereas an inappropriate combination can induce rapid trajectory deviations, preventing effective interaction. This phenomenon highlights the system's high selectivity with respect to "drift path controllability" and reflects the complex dynamics arising from multi-parameter regulation in nonlinear electric fields.

The intensity of the polarized electric field also has a substantial effect on the dynamical behavior of the spiral waves. The trajectory fluctuations of the spiral tips at different electric field intensities are shown in Fig. 11. The electric field frequency is set to $\omega = 2\omega_{\mathrm{spiral}}$, and the phase combination is fixed at $\phi_1 = 0$, $\phi_2 = \pi$, in order to isolate the effect of the electric field intensity.

At lower electric field intensities E_0, although the spiral waves can reach the critical distance required for interaction, they drift almost parallel along the perpendicular direction, preventing them from approaching closely enough to achieve annihilation. The trajectory distribution is very dense, as shown in Fig. 11(a), indicating that the drift velocity is extremely low and that the dynamical behavior is largely constrained by the weak electric field drive. When the intensity is increased to $E_0 = 0.09$ (Fig. 11(b)), the spiral waves are able to annihilate, showing that the electric field is sufficiently strong to induce effective interaction. However, the drift remains relatively slow, and the trajectories are still somewhat dense, indicating enhanced interaction without a significant increase in drift speed.

Increasing the intensity further to $E_0 = 0.10$ (Fig. 11(c)) significantly accelerates the drift of the spiral waves, demonstrating that the driving effect of the electric field on the spiral wave migration is enhanced. At this stage, the upward drift distance begins to shorten, reflecting more rapid mutual attraction and annihilation. When the intensity is raised to $E_0 = 0.11$ (Fig. 11(d)), the vertical drift distance is further reduced, and

the annihilation process is noticeably accelerated. Nevertheless, the overall trajectories remain nearly symmetric and circular without abrupt deviations, indicating that while the electric field has strengthened the driving force, it has not altered the migration direction of the spiral waves.

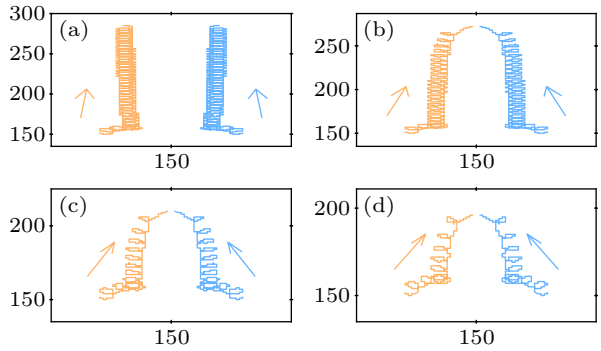


Fig. 11. Effect of polarized electric fields with different intensities on the annihilation of counter-rotating spiral waves. Mutual annihilation occurs only when $E_0 \geq 0.09$. The electric field intensities are (a) $E_0 = 0.08$, (b) $E_0 = 0.09$, (c) $E_0 = 0.10$, (d) $E_0 = 0.11$. The phase combination and frequency are fixed as $\phi_1 = 0$, $\phi_2 = \pi$, and $\omega = 2\omega_{\text{spiral}}$.

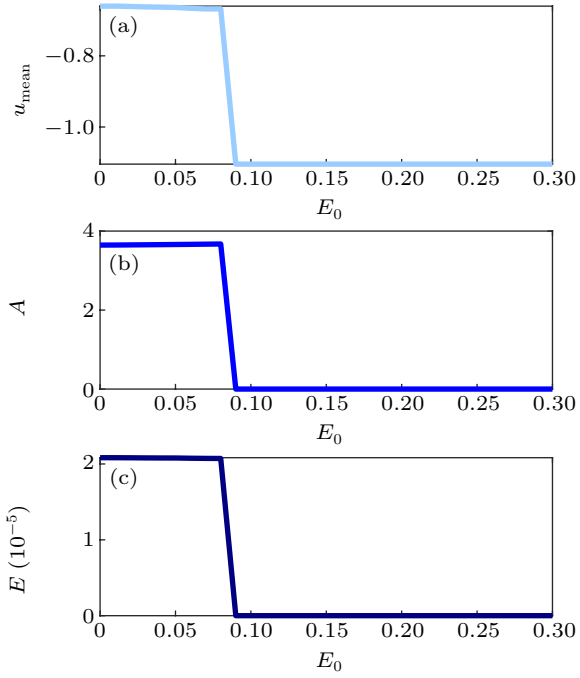


Fig. 12. Counter-rotating spiral waves can annihilate each other only when the electric field intensity reaches the threshold $E_0 = 0.09$. Variation of the following quantities with the electric field intensity E_0 is shown: (a) u_{mean}, (b) A, (c) E.

In summary, the intensity of the polarized electric field has a significant modulating effect on both the migration rate and the interaction strength of the spiral waves within a certain range. As the electric field intensity increases, its ability to drive the drift behavior of the spiral waves is enhanced, resulting in accelerated tip motion. Under weak electric field conditions, although the spiral waves can reach the critical distance required for interaction, the aggregation of the tips is slow due to insufficient driving, making annihilation difficult to achieve. In contrast, a stronger electric field drives the two spiral tips to approach rapidly along synergistic trajectories, thereby triggering synchronized annihilation more efficiently. This process demonstrates that the annihilation of spiral waves is highly dependent on the driving intensity of the electric field. Even after the tips reach the critical distance for short-range interaction, the polarized electric field remains essential for the realization of annihilation.

To further verify the effect of the intensity of the polarized electric field on spiral wave interactions, we investigated the variation of three statistics, u_{mean}, A, and E, with the electric field intensity E_0. Figure 12 illustrates the dependence of these three statistics on E_0. The results show that all three statistics exhibit abrupt changes at $E_0 = 0.09$, revealing the critical point at which the system undergoes annihilation. Only when the electric field intensity exceeds this critical value can the counter-rotating spiral waves approach sufficiently and achieve mutual annihilation. As shown in Fig. 12(a), u_{mean} undergoes a sudden drop at this point, indicating the occurrence of spiral wave annihilation. Figures 12(b) and 12(c) show that A and E decrease to lower levels almost simultaneously, further indicating that no node remains in an excited state.

For annihilation to occur, the two antichiral tips must first reach a critical spatial proximity. However, proximity alone is insufficient; a strong enough driving force is required to trigger the collapse of the activation front and the synchronized disappearance of the tips. The stronger the electric field, the faster the spiral waves drift and the more rapid and synchronized the approach of the two tips. When the driving force is insufficient, even closely spaced tips drift too slowly and couple too weakly to trigger effective annihilation.

The spiral tip trajectories at various angular frequencies ω are shown in Fig. 13. The angular frequencies of the polarized electric field were set to different multiples of the spiral waves' rotational frequency ω_{spiral}. Mutual annihilation occurs when the polarized electric field frequency is twice the spiral wave rotation frequency ($\omega = 2\omega_{\text{spiral}}$) (Fig. 13(e)). At this frequency, the spiral wave trajectories exhibit clear mutual attraction and merging, indicating effective resonant coupling between the applied field and the spiral wave dynamics. In contrast, when the field frequency does not match the spiral rotation frequency, the spiral waves remain mostly stationary or exhibit only weak perturbations (Figs. 13(b)–13(d) and 13(f)–13(h)), suggesting that the driving effect of the polarized electric field is weakened. When $\omega = 0$, the polarized electric field reduces to a constant field, and mutual annihilation can still occur (Fig. 13(a)).

In conclusion, the angular frequency of the polarized electric field significantly impacts the spiral wave dynamics. In particular, spiral waves exhibit stronger resonance responses and interaction ability when a specific relationship ($\omega = 2\omega_{\text{spiral}}$) exists between the external field frequency and

the spiral wave rotation frequency.

Whether annihilation occurs also depends on the initial state of the spiral waves. Figure 14 shows spiral wave trajectories under identical polarized electric field conditions ($\omega = 2\omega_{\text{spiral}}$, $E_0 = 0.10$, $\phi_1 = 0$, $\phi_2 = \pi$) for different initial phase combinations. Mutual annihilation occurs when the initial phases are $\theta_1 = \pi$, $\theta_2 = 0$ (Fig. 14(a)) and $\theta_1 = \frac{5\pi}{4}$, $\theta_2 = \frac{7\pi}{4}$ (Fig. 14(b)). In contrast, when the initial phases are $\theta_1 = \frac{3\pi}{2}$, $\theta_2 = \frac{3\pi}{2}$ (Fig. 14(c)) or $\theta_1 = \frac{7\pi}{4}$, $\theta_2 = \frac{5\pi}{4}$ (Fig. 14(d)), the spiral waves fail to approach closely and do not annihilate. Furthermore, after the phase combination (θ_1, θ_2) undergoes π-periodic variations, the annihilation state also exhibits periodic changes (Figs. 14(e)–14(f)). This indicates that spiral wave interactions are highly sensitive not only to the frequency and intensity of the electric field but also to the initial phase angles.

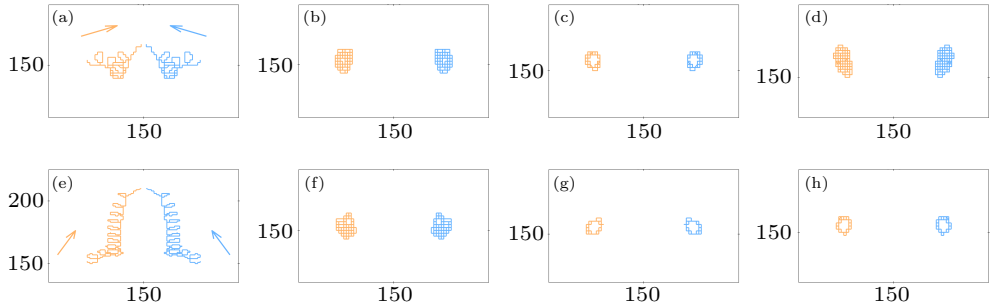


Fig. 13. Effect of different angular frequencies of the polarized electric field on the annihilation of counter-rotating spiral waves. The angular frequencies of the polarized electric field are (a) $\omega = 0$, (b) $\omega = 0.5\,\omega_{\text{spiral}}$, (c) $\omega = \omega_{\text{spiral}}$, (d) $\omega = 1.5\,\omega_{\text{spiral}}$, (e) $\omega = 2\,\omega_{\text{spiral}}$, (f) $\omega = 2.5\,\omega_{\text{spiral}}$, (g) $\omega = 3\,\omega_{\text{spiral}}$, (h) $\omega = 3.5\,\omega_{\text{spiral}}$, with $\phi_1 = 0$, $\phi_2 = \pi$, and $E_0 = 0.10$.

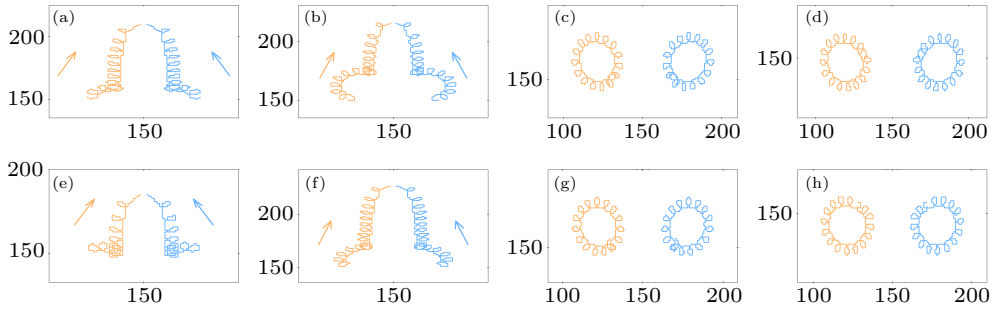


Fig. 14. Effect of a polarized electric field on the annihilation of counter-rotating spiral waves at different initial states. As the initial state of the spiral waves changes, the drift behavior exhibits periodic variations. The initial phases of the spiral waves are (a) $\theta_1 = \pi$, $\theta_2 = 0$, (b) $\theta_1 = \frac{5\pi}{4}$, $\theta_2 = \frac{7\pi}{4}$, (c) $\theta_1 = \frac{3\pi}{2}$, $\theta_2 = \frac{3\pi}{2}$, (d) $\theta_1 = \frac{7\pi}{4}$, $\theta_2 = \frac{5\pi}{4}$, (e) $\theta_1 = 0$, $\theta_2 = \pi$, (f) $\theta_1 = \frac{\pi}{4}$, $\theta_2 = \frac{3\pi}{4}$, (g) $\theta_1 = \frac{\pi}{2}$, $\theta_2 = \frac{\pi}{2}$, (h) $\theta_1 = \frac{3\pi}{4}$, $\theta_2 = \frac{\pi}{4}$, where θ_1 and θ_2 denote the initial phases of the left and right spiral waves, respectively. The polarized electric field parameters are $\phi_1 = 0$, $\phi_2 = \pi$, $E_0 = 0.10$, and $\omega = 2\,\omega_{\text{spiral}}$.

When the resonance condition (e.g., $\omega = 2\omega_{\text{spiral}}$) is satisfied between the driving frequency of the polarized electric field and the rotational frequency of the spiral waves, the electric field can stably drive the spiral waves to drift along a specific direction. Under this condition, if the initial phase difference between the two spiral waves is appropriate, the tip trajectories are guided centripetally, allowing them to enter the short-range interaction region. This facilitates the connection of the activation fronts and triggers synchronous collapse, ultimately resulting in mutual annihilation. Conversely, if the initial phase combination is unfavorable, the tip drift directions are spatially staggered, and even with sufficient electric field strength, the tips cannot effectively enter the interaction range, preventing annihilation. Therefore, orderly regulation of counter-rotating spiral wave annihilation can be achieved by selectively applying the polarized electric field in combination with precise tuning of the initial phase configuration of the spiral waves.

4. Discussion

This study employs the FitzHugh–Nagumo (FHN) model as the framework for local dynamics. Compared with complex myocardial tissue models, the FHN model has a simple structure, containing only two variables, u and v, while capturing the core dynamic characteristics of spiral waves with low computational cost. This choice enables systematic investigation of the regulatory effects of electric fields on spiral wave drift and annihilation in large-scale parameter scans and long-term simulations. Importantly, the use of a simplified model avoids interference from excessive physiological details, highlighting the universality of the mechanisms revealed. A large body of literature shows that patterns obtained from the FHN model are also relevant in more complex myocardial models and other excitable media. Therefore, the results of this study not only provide a theoretical basis for understanding spiral wave interactions under electric fields but also lay the foundation for future extension studies in real myocardial tissues and

three-dimensional scroll waves.

Higher-dimensional studies have shown a quantitative relationship between the stability spectrum of three-dimensional scroll waves and the drift characteristics of two-dimensional spiral waves.[57] This indicates that the dynamic properties of two-dimensional spiral waves are not only universal within their system but can also inform the understanding of three-dimensional spiral structures. Similarly, response functions have been shown to quantitatively and accurately predict drift velocities induced by external perturbations,[35,58] providing a solid theoretical foundation for dynamic control in two-dimensional systems. Additionally, applying an electric field to a stationary excitable medium can induce spherical waves around obstacles, with circularly polarized electric fields (CPEF) capable of generating spherical waves with frequencies higher than those of pinned scroll waves.[59] These theoretical and experimental findings underscore the diverse regulatory effects of electric fields on helical structures and provide essential context for exploring spiral wave interactions and annihilation mechanisms in two-dimensional systems.

Previous studies, such as those by Hu *et al.*, focused on the drift behavior of a single spiral wave driven by a polarized electric field in discontinuous myocardial tissue.[46] Pan *et al.* systematically investigated the regulatory effects of polarized electric fields, especially circularly polarized ones, on spiral wave behavior, including drift, frequency synchronization, and chiral symmetry breaking.[44] While foundational, these studies were primarily limited to single spiral waves or chiral breaking processes.

In contrast, this paper systematically investigates the interaction mechanisms between two counter-rotating spiral waves under various electric fields (DC, AC, and polarized). Our findings show that when the tips of two counter-rotating spiral waves are spatially separated, electric field-induced drift can gradually bring them into a critical proximity. Within this range, mutual attraction between the tips exceeds the effect of the electric field. As the tips approach further, the activation fronts form a spatially connected "zipper-like" structure that dynamically restricts independent tip motion, causing coordinated drift and ultimately leading to annihilation. This indicates that annihilation is driven not solely by the electric field but by the combined effects of the field and intrinsic tip attraction, revealing a mechanism distinct from previous studies.

Chiral-related interactions are ubiquitous across different material systems. For instance, in spinel chromites, spin-lattice coupling drives helical spin order with chirality-related magnetoelectric effects.[60] In tightly focused Laguerre–Gaussian beams, spin–orbit light interactions induce complex optical chirality distributions.[61] In ferroelectric GeS nanotubes, polarization reversal can exhibit chirality-coupled switching mechanisms.[62] These examples illustrate that chiral regulation is universal, extending beyond reaction-diffusion systems and inspiring interdisciplinary applications.

5. Conclusions

Based on the FitzHugh–Nagumo model, this study systematically investigates the effects of three types of electric fields — DCEF, ACEF, and PEF — on the interaction and annihilation of counter-rotating spiral waves. Simulations show that electric field parameters can significantly influence spiral wave drift direction, trajectory morphology, and interaction paths, enabling regulation of mutual attraction, proximity, and eventual annihilation.

Under a constant DC electric field, spiral wave drift depends on both the field direction and intrinsic chirality. DC fields drive spiral waves along the field direction, while chirality determines lateral drift. Synchronized annihilation occurs when two spiral waves approach within a short-range interaction distance under compatible chirality and drift direction. If the drift paths are opposed or staggered, annihilation cannot occur. This highlights the chiral selectivity induced by DC fields and their importance as a fundamental modulation tool.

AC electric fields affect spiral wave dynamics through phase, frequency, and intensity. Resonance occurs when the field frequency is close to twice the spiral rotation frequency, triggering strong directional drift and increasing the likelihood of effective spatial and temporal proximity. The field phase determines the initial drift direction and trajectory morphology, influencing whether tips can approach synergistically. Field intensity exhibits a threshold effect; below a critical value, drift occurs but annihilation is not achieved. Only above the critical intensity can synchronized annihilation occur, illustrating AC fields' capability for multilevel control via frequency, phase, intensity, and initial phase modulation.

Polarized electric fields regulate spiral wave dynamics in a more complex manner due to periodic rotation and multi-component superposition. Phase combinations significantly affect the maximum offset angle and overall trajectory displacement. Nonlinear polarization intensifies interactions, accelerating tip approach and annihilation. Continuous offset driven by the field ensures tips continue converging, leading to simultaneous annihilation. The process is highly sensitive to the initial state, particularly the spiral waves' initial phases. Therefore, precise control requires consideration of both field parameters and initial conditions to achieve synergistic regulation.

Although this study provides valuable insights within a two-dimensional model, actual biological tissues and material systems are often three-dimensional. Three-dimensional spiral waves, or scroll waves, extend two-dimensional spirals into 3D, rotating around filaments that can be straight, curved, or looped. These structures have more complex geometry and

dynamics. Future studies will extend to the three-dimensional FitzHugh–Nagumo model to explore electric field modulation of helical structures in 3D configurations.

Acknowledgments

This work was supported by the National Natural Science Foundation of China (Grant No. 12175080) and by Self-Determined Research Funds of Central China Normal University from the Colleges' Basic Research and Operation of MOE (Grant No. CCNU25JC012).

References

[1] Zaikin A N and Zhabotinsky A M 1970 *Nature* **225** 535
[2] Qu Z L, Hu G, Garfinkel A and Weiss J N 2014 *Phys. Rep.* **543** 61
[3] Davidenko J M, Pertsov A V, Salomonsz R, Baxter W and Jalife J 1992 *Nature* **355** 349
[4] Christoph J, Chebbok M, Richter C, Schröder-Schetelig J, Bittihn P, Stein S, Uzelac I, Fenton F H, Hasenfuß G, Gilmour R F and Luther S 2018 *Nature* **555** 667
[5] Jakubith S, Rotermund H H, Engel W, Von Oertzen A and Ertl G 1990 *Phys. Rev. Lett.* **65** 3013
[6] Winfree A T 1972 *Science* **175** 634
[7] Ouyang Q, Swinney H L and Li G 2000 *Phys. Rev. Lett.* **84** 1047
[8] Pandit S V and Jalife J 2013 *Circ. Res.* **112** 849
[9] Panfilov A V and Holden A V 1990 *Phys. Lett. A* **151** 23
[10] Gray R A, Jalife J, Panfilov A, Baxter W T, Cabo C, Davidenko J M and Pertsov A M 1995 *Circulation* **91** 2454
[11] Barać U, Perc M and Gosak M 2023 *Chaos* **33** 43120
[12] Majhi S, Perc M and Ghosh D 2022 *J. R. Soc. Interface* **19** 20220043
[13] Liu Y, Ma J, Xu Y and Jia Y 2019 *Int. J. Bifurc. Chaos* **29** 1950156
[14] Lu L L, Jia Y, Liu W H and Yang L J 2017 *Complexity* **2017** 1
[15] Ma J 2025 *Nonlinear Dyn.* **111** 25365
[16] Wu Y, Ding Q M, Li T Y, Yu D and Jia Y 2023 *Nonlinear Dyn.* **111** 2693
[17] Ding Q M, Wu Y, Li T Y, Yu D and Jia Y 2023 *Chaos Solitons Fractals* **171** 113464
[18] Ma J, Liu Q R, Ying H P and Wu Y 2013 *Commun. Nonlinear Sci. Numer. Simul.* **18** 1665
[19] Kai G 2025 *Eur. Phys. J. Spec. Top.* **234** 1051
[20] Yu D, Wang G W, Ding Q M, Li T Y and Jia Y 2022 *Chaos Solitons Fractals* **157** 111929
[21] Yu D, Zhan X, Yang L J and Jia Y 2023 *Phys. Rev. E* **108** 14205
[22] Yuan G Y, Xu L, Xu A G, Wang G R and Yang S P 2011 *Chaos Solitons Fractals* **44** 728
[23] Ramakrishnan B, Moroz I, Li C, Karthikeyan A and Rajagopal K 2021 *Eur. Phys. J. Spec. Top.* **230** 3369
[24] Ramakrishnan B, Karthikeyan A, Srinivasan A and Rajagopal K 2022 *Eur. Phys. J. Spec. Top.* **231** 2439
[25] Xia Y X, Zhi X P, Li T C, Pan J T, Panfilov A V and Zhang H 2022 *Phys. Rev. E* **106** 24405
[26] Hu Y P, Ding Q M, Wu Y, Jia Y, Li T Y, Yu D and Zhan X 2024 *Nonlinear Dyn.* **112** 19421
[27] Ding Q M, Hu Y P, Wu Y, Hu X Y, Jia Y and Yang L J 2025 *Chaos Solitons Fractals* **191** 115846
[28] Li T C, Zhong W, Ai B, Panfilov A V and Dierckx H 2022 *Phys. Rev. E* **105** 14214
[29] Sung Y L, Wang T W, Lin T T and Lin S F 2022 *Int. J. Arrhythmia* **23** 9
[30] Leemann S, Schneider-Warme F and Kleinlogel S 2023 *Pflüg. Arch. Eur. J. Physiol.* **475** 1421
[31] Ding Q M, Wu Y, Yu D, Li T Y and Jia Y 2023 *Phys. Lett. A* **489** 129154
[32] Malki G and Zlochiver S 2018 *Med. Eng. Phys.* **61** 69
[33] Steinbock O, Schütze J and Müller S C 1992 *Phys. Rev. Lett.* **68** 248
[34] Agladze K I and De Kepper P 1992 *J. Phys. Chem.* **96** 5239
[35] Li T C, Gao X, Zheng F F, Pan D B, Zheng B and Zhang H 2017 *Sci. Rep.* **7** 8657
[36] Muñuzuri A P, Gómez-Gesteira M, Pérez-Muñuzuri V, Krinsky V I and Pérez-Villar V 1994 *Phys. Rev. E* **50** 4258
[37] Chen J X, Zhang H and Li Y Q 2006 *J. Chem. Phys.* **124** 14505
[38] Luo J, Li T C and Zhang H 2020 *Phys. Rev. E* **101** 32205
[39] Zhang H, Hu B, Hu G and Xiao J H 2003 *J. Chem. Phys.* **119** 4468
[40] Deng L Y, Zhang H and Li Y Q 2009 *Phys. Rev. E* **79** 36107
[41] Cai M C, Pan J T and Zhang H 2012 *Phys. Rev. E* **86** 16208
[42] Ji L, Zhou Y, Li Q, Qiao C and Ouyang Q 2013 *Phys. Rev. E* **88** 42919
[43] Li B W, Deng L Y and Zhang H 2013 *Phys. Rev. E* **87** 42905
[44] Pan J T, He Y J, Xia Y X, Zhang H 2020 *Acta Phys. Sin.* **69** 80503 (in Chinese)
[45] Li T C, Li B W, Zheng B, Zhang H, Panfilov A and Dierckx H 2019 *New J. Phys.* **21** 43012
[46] Hu Y P, Ding Q M, Wu Y and Jia Y 2023 *Chaos Solitons Fractals* **175** 113957
[47] Li B W, Cai M C, Zhang H, Panfilov A V and Dierckx H 2014 *J. Chem. Phys.* **140** 184901
[48] Quail T, Shrier A and Glass L 2014 *Phys. Rev. Lett.* **113** 158101
[49] Kalita H and Dutta S 2022 *Phys. Rev. E* **105** 54213
[50] Ermakova E A, Pertsov A M and Shnol E E 1989 *Phys. Nonlinear Phenom.* **40** 185
[51] Kalita H, Khan P and Dutta S 2022 *Phys. Rev. E* **106** 34201
[52] He Y J, Li Q H, Zhou K S, Jiang R H, Jiang C Y, Pan J T, Zheng D F, Zheng B and Zhang H 2021 *Phys. Rev. E* **104** 014213
[53] Li T C, Pan D B, Zhou K S, Jiang R H, Jiang C Y, Zheng B and Zhang H 2018 *Phys. Rev. E* **98** 062405
[54] Li T C, Van Nieuwenhuyse E, Xia Y X, Pan J T, Duytschaever M, Knecht S, Vandersickel N, Zhou C S, Panfilov A V and Zhang H 2021 *Phys. Rev. E* **104** 64401
[55] Mermin N.D. 1979 *Rev. Mod. Phys* **51** 591
[56] Tyree T J, Murphy P and Rappel W J 2024 *Chaos* **34** 53131
[57] Henry H and Hakim V 2002 *Phys. Rev. E* **65** 46235
[58] Biktasheva I V, Barkley D, Biktashev V N and Foulkes A J 2010 *Phys. Rev. E* **81** 66202
[59] Pan D B, Gao X, Feng X, Pan J T and Zhang H 2016 *Sci. Rep.* **6** 21876
[60] Xu W, Lin G T, Shu M F, Jiao J L, Zhu J F, Ren Q Y, Le M D, Luo X, Sun Y P, Liu Y, Qu Z, Zhou H D, Gao S and Ma J 2024 *Chin. Phys. Lett.* **41** 117503
[61] Zhu M C, Fu S G and Man Z S 2023 *Chin. Phys. B* **32** 114202
[62] Wang H C, Wang Z H, Chen X Y, Wei S H, Zhu W and Zhang X 2023 *Chin. Phys. Lett.* **40** 47701